Laser Powder Bed Fusion Process Optimization of AlSi10Mg Alloy Using Selective Laser Melting: Dynamic Performance of Fatigue Behaviour, Microstructure, Hardness and Density

Mudda Nirish[*], R.Rajendra, Buschaiah Karolla
Department of Mechanical Engineering,
University College of Engineering (A), Osmania University,
Telangana, INDIA
[*]nirishyadav@gmail.com

ABSTRACT

The quality of a selective laser melting (SLM) component depends on build orientation and layer thickness, which are directly influenced by processing parameters. The present research of layer-by-layer additive simulation before starting the SLM process has several advantages, such as saving time, cost, and material. In this main investigation, the dynamic performance of fatigue strength, density, and hardness of AlSi10Mg alloy was produced by the SLM-AM according to the design of experiments. The L9 orthogonal array of the Taguchi method was created to perform the experimental development process. Finally, the obtained optimal process parameter with the highest values of fatigue strength, density, and hardness was found at a laser power of 225 Watts, a scan speed of 500 mm/s, and a hatching distance of 100 µm. The experimental density result was achieved with a high density value of 99.6% (2.66 g/cm^3) and a defect-free component and hardness of 126±5 HV. The future scope of this study will use optimal process parameters to find out mechanical properties for as built and preheated conditions for aerospace applications.

Keywords: *Selective Laser Melting; Geometric Dimensioning and Tolerance; Fatigue Strength; Microstructure; Density and Hardness*

ISSN 1823-5514, eISSN2550-164X

https://doi.org/10.24191/jmeche.v20i1.21074

Received for review: 2022-03-15
Accepted for publication: 2022-09-19
Published: 2023-01-15

Introduction

Selective laser melting (SLM), also called direct metal laser melting (DMLM), is a layer-by-layer manufacturing technology with fully dense and high-quality metal parts produced by the corresponding 3D computer-aided design (CAD) model [1]. The biggest drawback that limits the applicability of today's technologies is the high cost of AM components compared with conventional manufacturing process [2]. Metal AM provides the advantages of being flexible in terms of free geometric design and wasting less material in the SLM-AM process [3]. The current trend to increase productivity or efficiency is based on the process parameters of optimization technology, multi-laser machine process development, and automation aimed at reducing machine downtime and producing high-density parts [4]. To avoid defects in the SLM process maintain the minimum laser power and scan speed [5]. AM technology has built up within the defense, aerospace, and biomedical industries [6]. In SLM fabricated samples, three types of porosity are present: "lack of fusion", gas and shrinkage porosity, and key holing [7]. A "lack of fusion" is a bonding defect that arises in parts with a low energy density or low laser power [8]-[9]. Aluminum alloys are used common in aerospace application compared to titanium alloys because of AlSi10Mg alloy are easy to melt in SLM printing [10]. This SLM machine normally changes process parameters that can be improved AM part strength and performance [11]. The laser powder bed fusion (LPBF) systems have so many process parameters, mostly used for layer thickness, building direction, laser spot diameter, laser power, scan speed, and hatching distance [12]-[13].

Previous researchers have worked on the microstructure and mechanical properties of parts made of AlSi10Mg: powder properties [14], internal porosity of defective parts [15], hardness, surface roughness, and tensile properties [16]. From the literature survey, it was concluded that the mechanical properties, and particularly the fatigue strength of AlSi10Mg specimens [17], typically depend on internal microstructure, pores, porosity, cracks, and oxide films [18]. The various printing processes have process parameters that affect porosity on SLM-AM parts [19]. The build direction is main role in SLM printing; it can be concluded of AM part density [20]. The various process parameters that affect fatigue, microstructure, density, and hardness of AlSi10Mg alloy were discussed by giving process parameters such as the laser power, scan speed, hatching distance, and layer thickness [21]. The circulation of pores to parts in the AM printing depends on the building orientation. Specimens were displayed with low porosity and expressed with high fatigue performance in horizontal orientation [22]. The optimised parameters are empirically derived to generally produce dense materials, minimise defects, reduce surface roughness [23], increase build rate, and produce parts with acceptable material properties [24]. The process parameters provided by machine manufacturers are typically developed to

provide the best result in the material produced as a compromise of these competing (and interdependent) priorities [25].

In this work, optimization of process parameters with horizontal build orientation was conducted, and a test of bending fatigue test of AlSi10Mg parts manufactured by SLM was also conducted.

- Developed the additive process simulation for AM part using the design of experiment table.
- Using the Artec 3D scanner for geometric dimensioning and tolerance (GD&T) for geometric inaccuracy.
- To determine mechanical properties of fatigue strength, hardness, density and microstructure characterization.
- The output dynamic performance is considered as a prediction of fatigue strength.
- Used the Taguchi method for output statistical evaluation.

Experimental Procedure

Material

The laser power melted AlSi10Mg aluminium alloy printed specimens for fatigue tests were fabricated by the SLM process. Table 1 shows the chemical composition of AlSi10Mg.

Table 1: Chemical composition of AlSi10Mg alloy (www.slm solutions.com)

Al	Si	Fe	Cu	Mn	Mg	Zn	Ti	Ni	Pb	Sn	Other total
Bal.	9 – 11	.55	.05	.45	.20 – .45	.10	.15	.05	.05	.05	.15

Specimen design

The SLM samples were prepared for fatigue strength as per the ASTM standard E2948 and the specimen dimensions were 130 mm in length with an 11diameter, gauged at 40 mm in length with a 7.5 mm diameter, and a radius of 7.5 mm as shown in Figure 1.

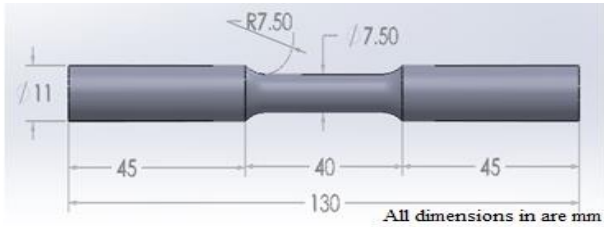

Figure 1: Test specimen size and its dimension considered fatigue testing line diagram

Powder analysis

The power particle size distribution has the main importance in the SLM process because it has the main influence on the part qualification, such as performance. The powder particle size distribution ranged from 20 to 63 µm and was supplied by SLM Solution Group AG, Germany. The powder weighted residual is 0.694%, the specific surface area is 0.154 m^2/g, the surface weighted mean is 38.8 µm and the volume weighted mean is 43.505 µm as shown in Figures 2a and 2b.

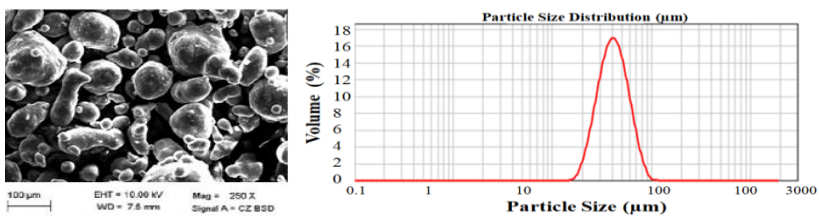

(a) (b)

Figure 2: a) SEM particle analysis, and b) powder particle size distribution

SLM process

This is mostly due to the high cost of the equipment parts being manufactured and operating SLM process parameters in three zones. Lack of fusion (the most common cause for concern; insufficient laser energy density, poor laser parameters, poor hatching strategy, spatter particles), key holing (a common cause for concern and too high laser energy density) and balling (not commonly, usually found only during parameter development and trying to get too fact). The SLM process parameter optimization includes laser power (LP or P), layer thickness (LT or t), beam diameter (D), material feed (mp), hatching distance (HD or h), scan speed (SS or v), building directions (BD or d) (X, Y, and Z axes) and SLM line diagram as shown in Figure 3a.

These are the adjustable parameter layer thickness, laser power, scanning speed, hatch spacing, and recoater speed as shown in Figure 3b.

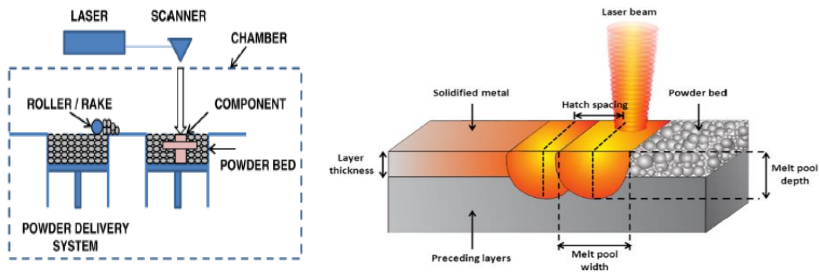

(a) (b)

Figure 3: a) SLM schematic diagram, and b) printing process (www. slm-solutions.com)

All the specimens were fabricated for the optimization of process parameters using the Taguchi L9 orthogonal array (OA) by producing an SLM machine M280 model of the AlSi10Mg alloy. The powder particle distribution used in our experiments ranged from 20 to 63 µm. The SLM build platform dimensions are 280 × 280 × 365 mm and uses a continuous IPG fiber laser. In this study, the process parameters that varied were laser power at three levels: 200, 225, and 250 Watts; scan speed at three levels: 400, 500, and 600 mm/s; and hatch distance at three levels: 60, 80, and 100 m. The remaining process parameters are kept constant as a laser spot diameter of 75 µm, layer thickness of 30 µm, build platform temperature of 150 ºC, and a scanning pattern of 0°. All the specimens were built in a horizontal orientation (i.e., without any support structure) and used only printing support on the SLM base plate (i.e., block support structure). Maintain the atmosphere in the SLM printing process at a maximum oxygen content level of 0.12%. The process parameters were considered as per design of experiment and an L9 (3^3) OA as shown in Tables 2 and 3.

Table 2: Levels and their factors for LPBF of AlSi10Mg alloy

Process Parameters	Level 1	Level 2	Level 3
A: Laser power (LP) in Watts	200	225	250
B: Scan speed (SS) in mm/s	400	500	600
C: Hatching distance (HD) in µm	60	80	100

Table 3: used L9 orthogonal array as per design of experiment

Trials	Laser power (Watts)	Scan speed (mm/sec)	Hatching distance (µm)
Trial (T1)	200	400	60
Trial (T2)	200	500	80
Trial (T3)	200	600	100
Trial (T4)	225	400	80
Trial (T5)	225	500	100
Trial (T6)	225	600	60
Trial (T7)	250	400	100
Trial (T8)	250	500	60
Trial (T9)	250	600	80

The SLM additive designer's inbuilt software was used to generate individual process parameters based on a given design of experiment, and the data was then transferred to an SLM machine for printing process, as shown in Figure 4a. The laser energy density was calculated by Equation (1) and density values as shown in Figure 4b.

$$E = P / s \times h \times t \tag{1}$$

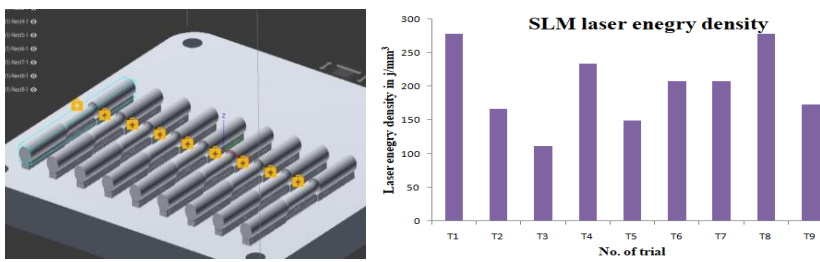

(a) (b)

Figure 4: a) Layout of specimen on SLM 280 build platform and b) Laser energy density value by Taguchi L9 OA

After given .stl file to the SLM printing process based on the process parameters and also calculated the laser energy density according to L9 OA.

Results and Discussion

Previous researchers have worked on the microstructure and mechanical properties of parts made of AlSi10Mg: powder properties, internal porosity of defective parts, hardness, surface roughness, and tensile properties. This research worked on fatigue strength improvement based on the given process parameter optimisation [12], which also increased the life cycles of SLM-AM parts [16].

Simulation of part using experimental design table

The Altair Inspire 3D software used for AM part thermal gradient in SLM printing Process. Temperature is the main important process in the SLM printing process and it is also done thermal analysis simulation (i.e., saving cost, time and material) to optimise the process parameter used for the L9 parameter before SLM print as shown in Figure 5a (displacement) and Figure 5b (temperature ranges). From the simulation results, trial 5 produced better results, with less temperature and less displacement. This parameter is considered to avoid defects and thermal displacement as shown in Figure 6a and temperature range as shown in Figure 6b. If a part was printed at a high temperature, it required a high cooling rate and produced defects with thermal defects (i.e., inaccurate geometry [4]).

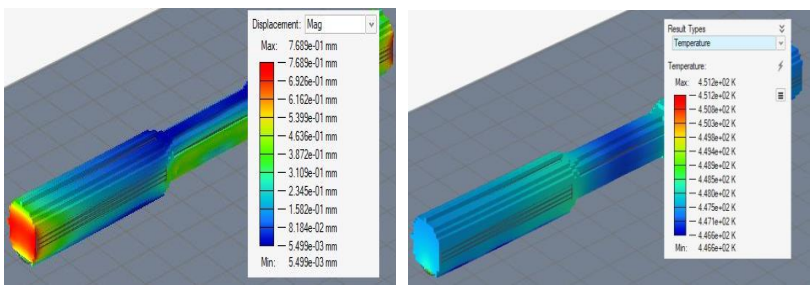

(a) (b)

Figure 5: a) Thermal simulations of displacement, and b) SLM printing temperatures used in printing process

Geometric accuracy of part

As shown in figure 7a, the measured geometric dimensions for part geometry inaccuracy were achieved using an Artec 3D scanner with a high-resolution white laser. The technology used in this research scanned the SLM manufactured parts and observed the geometric shape (such as thermal distortion and deviation, i.e., geometry inaccuracy) [4]. From figure 7b scanned all the specimens after SLM manufactured and also compared the dimensions of the nominal diameter with the SLM printed diameter.

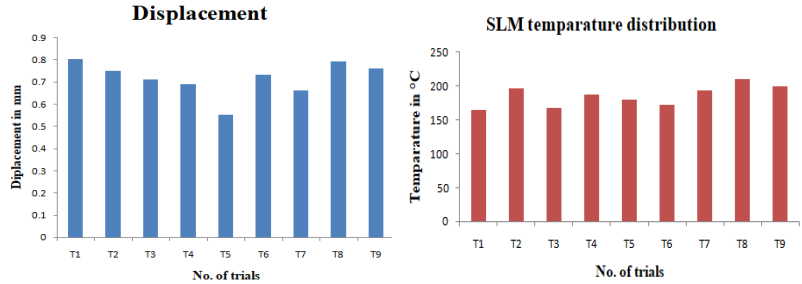

(a) (b)

Figure 6: a) Thermal analysis of displacement, and b) SLM printing process temperature

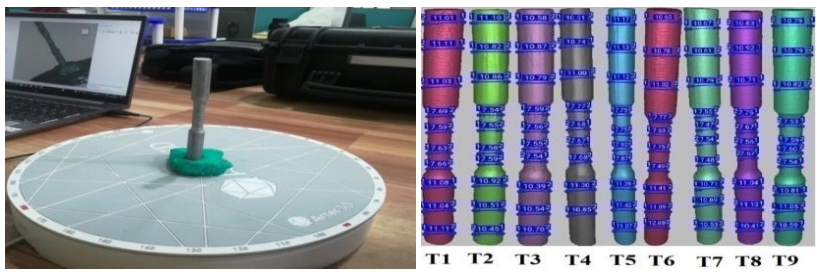

(a) (b)

Figure 7: a) Artec 3D scanning for part geometry and part printed is located, and b) scanned diametrical deviation of top, middle and lower diameter section (T5 part give dimensionally accurate geometry)

The given design diameters of gauge were 7.5 mm in diameter with a 40 mm length at the top and bottom, and 11 mm in diameter with a 45 mm length. The entire specimen diameter (bottom, top, and gauge) was increased due to the high laser with low scan rate as shown in Figures 8a and 8b. Except for Trial5, all of the specimens have geometric inaccuracy due to various process parameter effects.

Dynamic performance of AM part-fatigue testing

Dynamic bending fatigue performance is more important for applied dynamic load on aerospace components. It is well known that the fatigue strength of AlSi10Mg alloys depends on metallurgical defects and porosity effects in oxide layer films. The fatigue performance was conducted in a fully reversed with rotating bending mode. The experiment was conducted as a fatigue test at room temperature on the motor with a driven shaft rotating beam machine. The machine components are: flexible bearing, weight hanger assembly,

bearing spindle (shaft), bearing and its housing assembly, chuck, digital counter, AC electric motor as shown in Figure 9a and after SLM manufactured test specimens for fatigure testing as shown in Figure 9b.

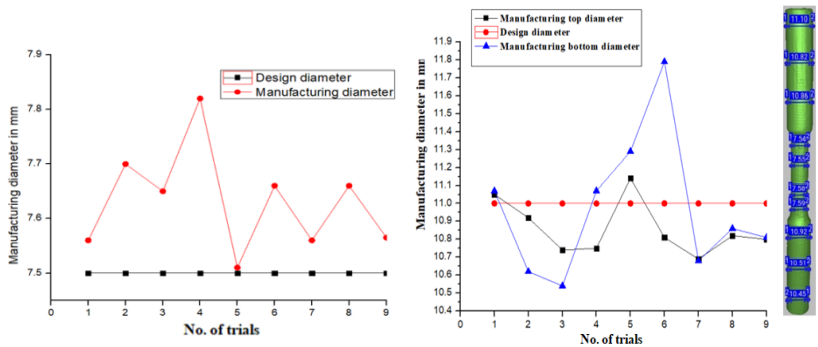

(a) (b)

Figure 8: (a) and, (b) compared the diameters with design diameter

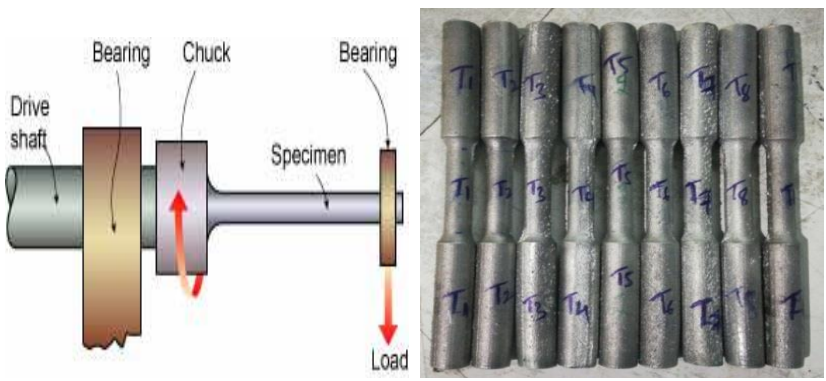

(a) (b)

Figure 9: a) Fatigue testing machine, and b) SLM manufactured parts

From the Figure 9b after SLM manufcatured sample for fatigue tesing as per design of experiments like Trial 1 to Trial 9 and calculated the fatigue life cycles for 3D printed samples. A typical fatigue test piece has three areas: a test section and two grip clamps or ends. The grip hold ends are designed for load transfer from the test machine hold to the test section and can be identical, especially in rotary bending fatigue tests. To eliminate any stress concentrations in the transition from the grip ends to the test region, broad, smoothly blended radii are used. The design and type of test piece used depends on the fatigue tester used and the purpose of the fatigue test.

The test section of the specimen should be sized to take the fatigue load capacity with a reduced cross section to prevent damage to the clamp ends from sample failure. The conducted test for all specimens was obtained as a process parameter at a particular constant load, i.e., a stress amplitude of 10 Kg, or 145.14 MPa [16]. The prediction of fatigue life at applied constant load and calculating the motor rpm at braked of the specimen as shoen in figure 10a, then get the number of cycles ploted as shown in Figure 10b.

- The motor rpm is 2880. 1 minute is equal to 2880 rev (i.e., 1 sec = 2880/60 = 48 rps).
- The number of cycles is equal to the time taken (s) × 48 rps.
- The prediction of the fatigue strength calculation:
  The length of the shaft (L) is 490 mm.
  The diameter of the shaft (d) is 15 mm, and
  For the fatigue test, a load of 10 Kg is applied.
- Weight (W) = 10 × 9.81 = 98.1 N.
- Bending moment, M

$$M = W \times L \tag{2}$$

$= 98.1 \times 490$

$= 48069$ N-mm and

- Bending stress, (σ_b)

$$\sigma b = 32M / \pi d^3 \tag{3}$$

$= 32 \times 48069 / 3.14 \times (15)^3$

$= 145.14$ MPa.

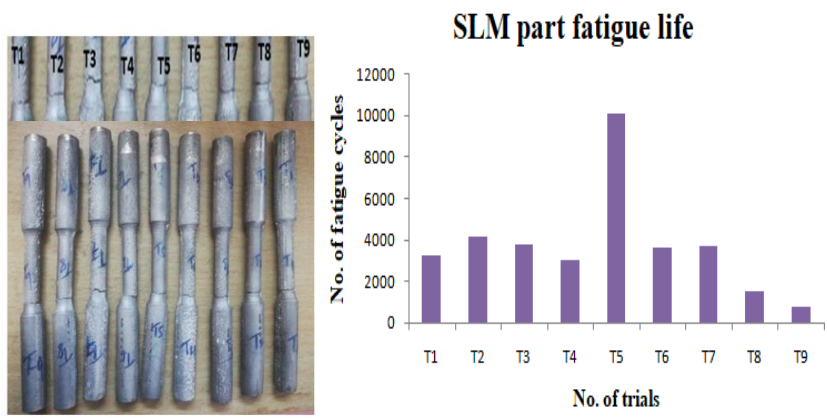

(a) (b)

Figure 10: a) After fatigue tested breaked specimens, and b) results

From Figure 10b, which shows fatigue life cycles for each specimen using constant loads. The fatigue life also depends on the process parameters,

like when using the high and low range parameters, a lot of pores, oxide films, and cracks are formed when using low laser power with scan speed (trai 1, trial 2, and trial 3), and there is also thermal deviation when using high laser power with scan speed (trai 7, trial 8, and trial 9). The trial 5 achieved high fatigue cycles because of geometric accuracy and no metalurgical defects.

Hardness and density

The hardness and density results according to design of experiment L9 OA are shown in Figures 11a and 11b. The hardness and mechanical property values are mainly dependent on the microstructure of pores, cracks, and porosity with thermal deviation. When used, the high laser power and low scan speed due to keyholing of high energy densities Vickers hardness was determined through microhardness testing, with each specimen having an average of three indentations in three different areas. The highest value of hardness achieved was 126±5 HV [6] under a load of 1000 grams with a 10 second duration. The prepared the samples for density testing by the Archimedes standard principle, which is used by xylene water. The theoretical density of AlSi10Mg alloy powder (ρt) is 2.67 g/cm^3 and, after SLM, manufactured parts have the highest density of 2.66 g/cm^3. According to the graph, increasing the laser power from 200 to 250 Watts and the scan speed from 400 to 600 mm/s reduced the density from 99.9% to 95% and the hardness from 126±5 to 96±5 HV compared with literature survey [5], [9]. It shows that the optimum value of hardness and density occurred at trial 5.

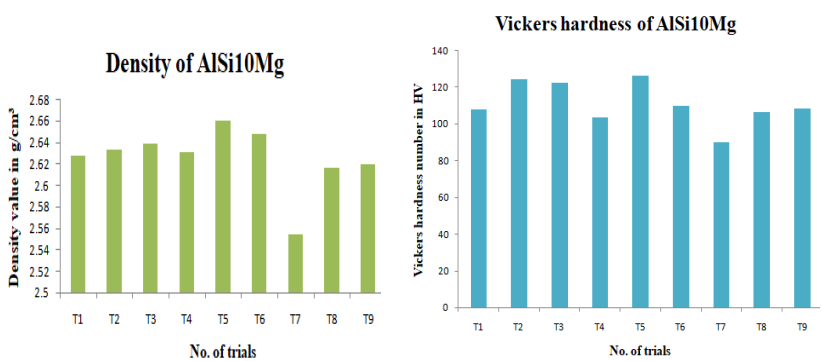

(a) (b)

Figure 11: a) Vickers hardness, and b) density of AlSi10Mg samples

Microstructure evaluation

The scanning electron microscope (SEM) was used for microstructure characterization at the different magnification levels as shown in Figures 12a,

12b, and 12c. As shown in Figures 12d, 12e, and 12f, a lot of pores, oxide films, and cracks are formed when using low laser power with scan speed (trai 1, trial 2, and trial 3), and there is also thermal deviation when using high laser power with scan speed (trai 7, trial 8, and trial 9). In terms of strength and performance, the hatching distance was the most important factor. The pores can be divided into spherical pores and irregular pores. Cracks are observed along with the horizontal direction of the structure. Due to the poor wettability of oxides and metals, long cracks were formed and spread along the surface. Due to the low cooling rate, some of the AlSi10Mg powder particles are formed as a result of oxidation during the SLM process. The decrease in laser power, density, and hardness also decreased. The increase in san speed then hardness increased and density decreased due to porosity.

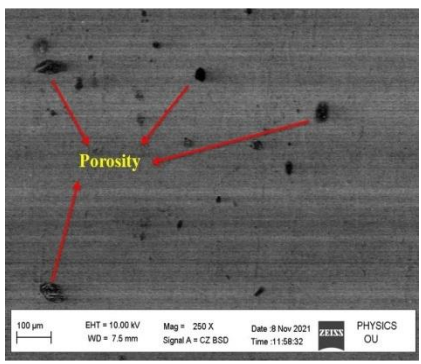

(a)

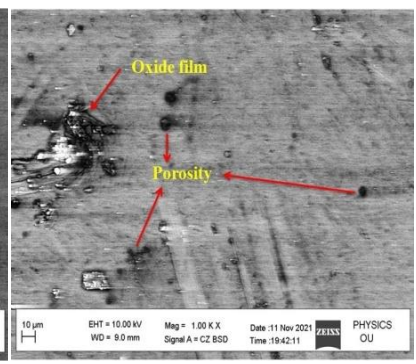

(b)

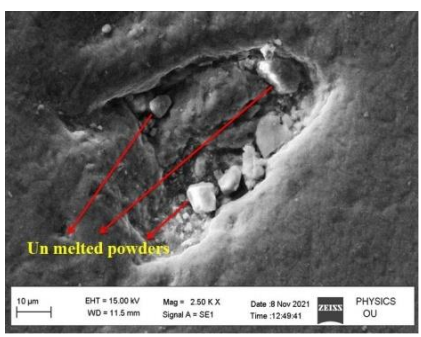

(c)

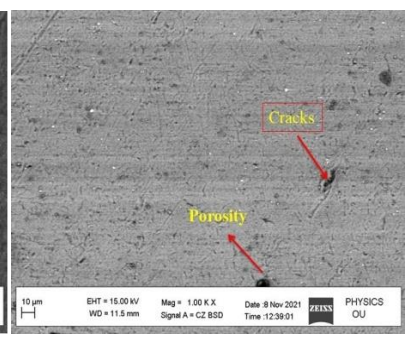

(d)

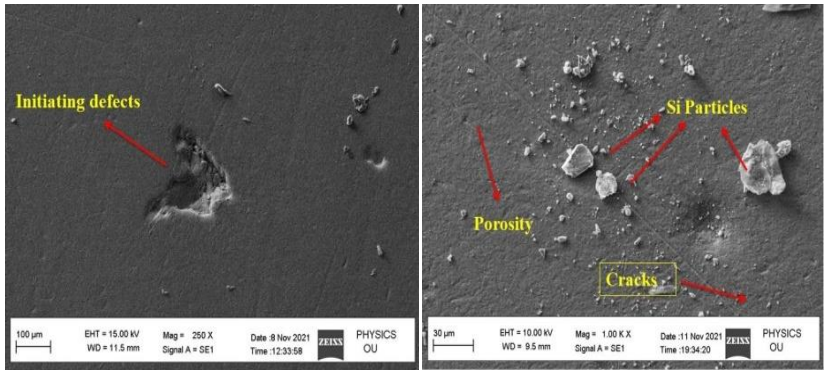

(e) (f)

Figure 12: Defects at different laser power and scan rates; (a) 200 watts with 400 mm/s, (b) 200 watts with 500 mm/s, (c) 200 watts with 4600 mm/s, (d) 250 watts with 400 mm/s, (e) 250 watts with 500 mm/s, and (f) 250 watts with 600 mm/s

From the design of experiment manufactured sample trial 5, all achieved full density and without defects, shown at different magnifications as shown in Figures 13 and 14. The microstructural characterization had the main influence on mechanical properties like strength and hardness.

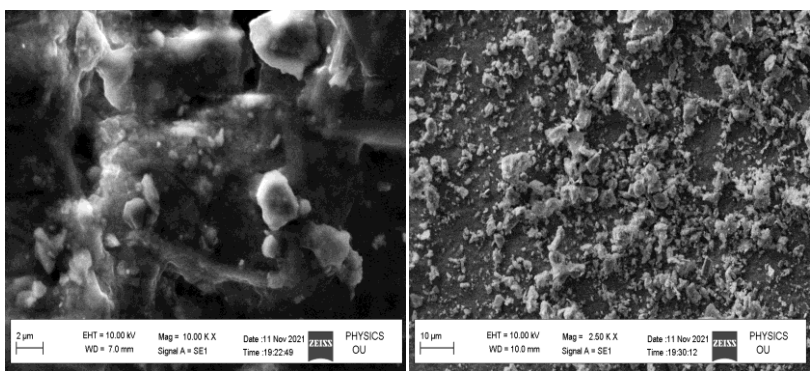

(a) (b)

Figure 13: (a) and, (b) defects free components at 225 watts with 500 mm/s

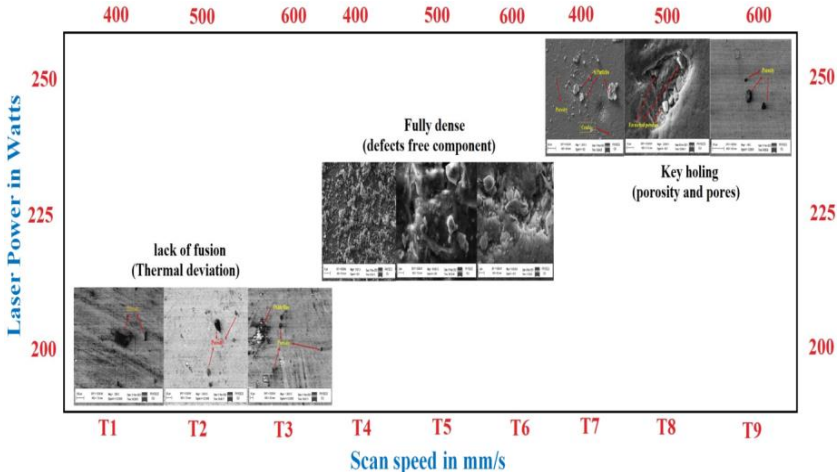

Figure 14: Comparison of laser power with scan speed microstructure evaluation

Taguchi Method

Design of experimental

The Taguchi technique uses experimental results to optimise the process parameters and can be classified into the following steps:

- To design and run the experiment as 3^3 (L9).
- Give the process parameters of levels and factors.
- Next, using the signal-to-noise ratio (S/N) and analysis of variance.
- Examine the experimental design (ANOVA).
- Finally, it receives the optimal process parameters based on the analysis results.

Signal-to-noise (S/N) ratio

In this method, the experimental results for the S/N ratio were considered the higher value (i.e., fatigue strength, density, and hardness). The best way to apply the condition rule to a larger S/N ratio is to use the following Equation (4).

$$S/N = -10 \log \left[\frac{1}{n} \sum_{i=1}^{n} \frac{1}{y_i^2} \right] \quad (4)$$

Where n is the total number of experiments, y_i^2 is the density value for ith experiment, and Taguchi analysis considers the highest number of cycles

(trial 5). From the response table delta statistic, the highest factor rank for laser power is 1, scan speed is rank 2, and hatching distance is rank 3.

Analysis of Variance (ANOVA)

Analysis of variance (ANOVA) is the most frequently used statistical method. In this case, ANOVA was required to determine the contribution of each process parameter to fatigue strength. In ANOVA, the sum of squares (SST), the sum of squares of each factor (SSF), the mean square of each factor (MSF), the degree of freedom (DF), percentage of the contribution (%), P-test, and F-test were calculated by the regression analysis of various process parameters such as laser power, scan speed, and hatching distance. To determine which level of each element provides the best performance and results, levels with values from response table 4 were used. From Figure 15, it is clear that laser power is the most influential factor, followed by scan speed and hatching distance. The slope line was connected at various levels with the process parameters of each variable. A laser power of 225 Watts (A2), a scan speed of 500 mm/s (B2), and a hatching distance of 100 m (C3) were used to achieve the optimal process parameter for fatigue strength.

Table 4: Statistical method used by ANNOVA

Source	DF	Seq SS	Contribution	Adj SS	Adj MS	F-Value	P-Value
Regressi	3	2006853	40.04%	2006853	668951	0.60	0.641
Laser Power in Watts	1	1175440	25.74%	1175440	117544	1.06	0.350
Scan Speed in mm/s	1	228931	15.39%	228931	228931	0.02	0.891
Hatching Distance in µm	1	8085204	12.39%	8085204	808520	0.73	0.432
Error	5	5544076	6.44%	554407	11088		
Total	8	7550930	100.00%				

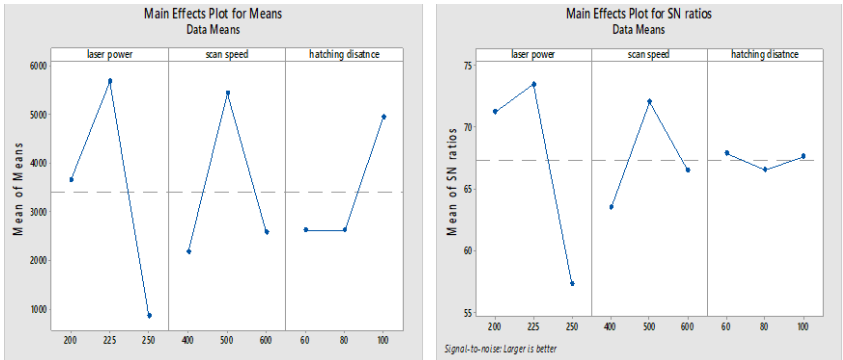

(a) (b)

Figure 15: S/N ratio graph for fatigue strength

Conclusion

This research analysed the defects using various process parameters and found their dynamic performance of highest fatigue strength. In this SLM process, the part build orientation is the most important factor, especially in fatigue performance.

i. It is observed that when using a high laser at the different scan speeds in the SLM process, the additive simulation results are given the AM part displacement (i.e., deviation of geometric defects) due to high laser power [4]. For high density and mechanical strength, it is preferable to consider values such as low laser power with a lower scan speed rate.

ii. A very high SS of 600 mm/s was given a high percentage of porosity, pores, and cracks, i.e., resulting in a drastic reduction in fatigue strength, density, and hardness. The hardness was decreased due to increasing the scan speed rate from 400 to 600 mm/s and the density was decreased due to increasing the laser power from 200 to 250 watts. The porosity depends on the complete scan rate [9].

iii. Finally, achieved a defect-free component without distortion at laser power of 225 Watts, scan speed of 500 mm/s, and hatching distance of 100 µm [12]. The laser energy density at trial (t5) was 150 J/mm^3. The obtained results at t5: fatigue life cycle was 1.08×10^4 (applied stress amplitude of 145.14 MPa) [16], density was 2.66 (99.6%), and hardness was 126±5 HV (applied 1000 grams with a 10 second hold at three different areas).

iv. After using experimental results with a statistical method (ANOVA), it was observed that the most significant parameter was

laser power, which had a contribution of 25.74%, scan speed was 15.39%, and hatching distance was 12.39%.

v. The future scope of this study using optimal process parameters to find out mechanical properties for as-build and preheated conditions for aerospace application.

Contribution of Author

Conceptualization: Mudda Nirish , R.Rajendra; Methodology, Mudda Nirish, R.Rajendra, Buschaiah Karolla.; Software, Mudda Nirish; Formal analysis, Mudda Nirish, Buschaiah Karolla; Investigation, Mudda Nirish, R.Rajendra; Data curation, Mudda Nirish, R.Rajendra; Writing—original draft preparation, Mudda Nirish; Writing—review and editing, Mudda Nirish, R.Rajendra and Buschaiah Karolla; Visualization, Mudda Nirish; Supervision, R.Rajendra.; Funding acquisition, Mudda Nirish. All authors have read and agreed to the published version of the manuscript.

Funding

This research received no external funding.

Conflict of Interests

This research received no Conflict of interests.

Acknowledgement

The authors would like to thank the research facilities centre funded by the Govt. of India's Rashtriya Uchchatar Shiksha Abhiyan (RUSA 2.0) at the University College of Engineering (A), Osmania University, Hyderabad, India.

Nomenclature

W	Wight or Load
l	Length of Shaft
d	Diameter of Shaft
σ_b	Bending Stress
M	Bending Moment
n	Total Number of Experiments
y_i^2	Density Value for i^{th} Experiment
E	Laser Enegry Density
P	Laser Power
v	Scan Speed
h	Hatching Distance
t	Layer Thickness

Abbreviation

FEM	Finite Element Method
S/N	Signal-to-Noise
ANOVA	Analyses Of Variance
AM	Additive Manufacturing
DMLM	Direct Metal Laser Melting
SLM	Selective Laser Melting
LPBF	Laser Powder Bed Fusion
CAD	Computer Aided Design
DoE	Design of Experiments
SST	Sum of Squares
SSF	Sum of Squares of Each Factor
MSF	Mean Square of Each Factor
GD&T	Geometric Dimensioning and Tolerance
SEM	Scanning Electron Microscope

References

[1] Shahrubudin N, Lee TC, Ramlan R, "An overview on 3D printing technology: Technological, materials, and applications," *Procedia Manufacturing*, vol. 35, pp. 1286-96, 2019.

[2] Frazier WE, "Metal additive manufacturing: a review," *Journal of Materials Engineering and performance*, vol. 23, no. 6, pp. 1917-28, 2014.

[3] Nirish M and Rajendra R, "Suitability of metal additive manufacturing processes for part topology optimization–A comparative study," *Materials Today: Proceedings,* vol 27, pp.1601-7, 2020.

[4] Wang P, Lei H, Zhu X, Chen H, Fang D, "Influence of manufacturing geometric defects on the mechanical properties of AlSi10Mg alloy fabricated by selective laser melting," *Journal of Alloys and Compounds*. vol.789, pp. 852-859, 2019.

[5] Mudda Nirish and R.Rajendra, "Optimization of Process Parameter and Additive Simulation for Fatigue Strength Development by Selective Laser Melting of AlSi10Mg Alloy," *International Journal of Mechanical Engineering*, vol. 7, no. 2, pp. 3795-3802, 2022.

[6] Liu Y, Liu C, Liu W, Ma Y, Tang S, Liang C, Cai Q, Zhang C, "Optimization of parameters in laser powder deposition AlSi10Mg alloy using Taguchi method," *Optics & Laser Technology*, vol. 111, pp. 470-80, 2019.

[7] Read N, Wang W, Essa K, Attallah MM, "Selective laser melting of AlSi10Mg alloy: Process optimisation and mechanical properties development," *Materials & Design*, vol. 65, pp. 417-24, 2015.

[8] Mudda Nirish and R.Rajendra, "Heat Treatment Effect on the Mechanical Properties of AlSi10Mg Produced by Selective Laser Melting," *Journal of Mechanical Engineering Research and Development*, vol. 45, no. 2, pp. 19-28, 2022.

[9] Wu H, Li J, Wei Z, Wei P, "Effect of processing parameters on forming defects during selective laser melting of AlSi10Mg powder," *Rapid Prototyping Journal*, vol. 26, no. 5, pp. 871-879, 2020.

[10] Oliveira JP, LaLonde AD, Ma J, "Processing parameters in laser powder bed fusion metal additive manufacturing," *Materials & Design*, vol.193, pp. 108762, 2020.

[11] Bajaj P, Wright J, Todd I, Jägle EA, "Predictive process parameter selection for Selective Laser Melting Manufacturing: Applications to high thermal conductivity alloys," *Additive Manufacturing*, vol. 27, pp. 246-58, 2019.

[12] Mudda Nirish and R.Rajendra, "Additive Layer by Layer Simulation and Taguchi Loss of Function for AlSi10Mg Alloy Samples Manufactured by Selective Laser Melting," International Journal of Mechanical Engineering, vol. 7, no. 5, pp. 765-770, 2022.

[13] Beretta S, Gargourimotlagh M, Foletti S, Du Plessis A, Riccio M, "Fatigue strength assessment of "as built" AlSi10Mg manufactured by SLM with different build orientations," *International Journal of Fatigue*, vol. 139, pp. 105737, 2020.

[14] Mudda Nirish and R.Rajendra, "Effect of Heat Treatment on Wear Characterization of AlSi10Mg Alloy Manufactured by Selective Laser Melting," Journal of Mechanical Engineering Research and Development, vol. 45, no. 2, pp. 10-18, 2022.

[15] Xu ZW, Wang Q, Wang XS, Tan CH, Guo MH, Gao PB, "High cycle fatigue performance of AlSi10mg alloy produced by selective laser melting," *Mechanics of Materials*, vol. 148, pp. 103499, 2020.
[16] Mudda Nirish and R.Rajendra, "Additive Simulation and Process Parameter Optimization for Wear Characterization Development by Selective Laser Melting of AlSi10Mg Alloy," *Journal of Characterization*, vol. 2, no. 2, pp. 103-116, 2022.
[17] Qian G, Jian Z, Qian Y, Pan X, Ma X, Hong Y, "Very-high-cycle fatigue behavior of AlSi10Mg manufactured by selective laser melting: Effect of build orientation and mean stress," *International Journal of Fatigue*, vol. 138, pp. 105696, 2020.
[18] Mudda Nirish and R.Rajendra, "Fatigue Performance Improvement of AlSi10Mg Manufactured by Selective Laser Melting through Heat Treatment," *Journal of Mechanical Engineering Research and Development*, vol. 45, no. 3, pp. 01-13, 2022.
[19] Santos LM, Ferreira JA, Jesus JS, Costa JM, Capela C, "Fatigue behaviour of selective laser melting steel components," *Theoretical and Applied Fracture Mechanics*, vol. 85, pp. 9-15, 2016.
[20] Uzan NE, Ramati S, Shneck R, Frage N, Yeheskel O, "On the effect of shot-peening on fatigue resistance of AlSi10Mg specimens fabricated by additive manufacturing using selective laser melting (AM-SLM)," *Additive Manufacturing*, vol. 21, pp. 458-64, 2018.
[21] Jian ZM, Qian GA, Paolino DS, Tridello A, Berto F, Hong YS, "Crack initiation behavior and fatigue performance up to very-high-cycle regime of AlSi10Mg fabricated by selective laser melting with two powder sizes," *International Journal of Fatigue*, vol.143, pp.106013, 2021.
[22] Mudda Nirish and R.Rajendra, "Optimization Process Parameter on Wear Characterization of Al6061 and AlSi10Mg Alloy Manufactured by Selective Laser Melting," *International Journal of 3D Printing and Additive Manufacturing*, vol. 2, no. 1. pp. 1-10. 2022.
[23] Brandl E, Heckenberger U, Holzinger V, Buchbinder D, "Additive manufactured AlSi10Mg samples using Selective Laser Melting (SLM): Microstructure, high cycle fatigue, and fracture behavior," *Materials & Design*. vol. 34, pp.159-69, 2012.
[24] Zhao J, Easton M, Qian M, Leary M, Brandt M, "Effect of building direction on porosity and fatigue life of selective laser melted AlSi12Mg alloy," *Materials Science and Engineering: A*, vol. 729, pp. 76-85, 2018.
[25] Nirish M, Rajendra R. "Selective laser melting process parameter simulation and topology optimization by aerospace component of AlSi10Mg alloy," *InAIP Conference Proceedings 2022*, vol. 2648, no. 1, pp. 020019, 2022.